Analytical all-induction state model for wind turbine wakes

N. Bempedelis and K. Steiros*
Department of Aeronautics, Imperial College London, London SW7 2AZ, United Kingdom

(Received 14 September 2021; accepted 18 March 2022; published 31 March 2022)

Analytical wind turbine wake models are an integral component of wind farm design and optimization. However, when the turbine induction factor increases, these models are prone to failure, as they do not account for the increasingly important effects of low wake pressure. To resolve this issue, this paper proposes an analytical wake model which incorporates the effect of wake pressure in its predictions. The model is based on inviscid flow theory for the initial wake region [K. Steiros and M. Hultmark. J. Fluid Mech. **853**, R3 (2018)] and an extension of Morton's [B. R. Morton. J. Fluid Mech. **10**, 101 (1961)] theory for the far wake, both of which include the effects of wake pressure. Comparison with high-fidelity wind turbine simulations shows that the model is comparable to conventional ones at low induction factors, but continues to be accurate at higher induction factors where existing models break down.

DOI: 10.1103/PhysRevFluids.7.034605

I. INTRODUCTION

Analytical wake models are tools that predict the velocity deficit downstream of a wind turbine, and ultimately the flow within a wind farm. These models play a pivotal role in the design and optimization of wind farm control and layout due to their simplicity, low cost, and practicality [1,2]. As a result, a large number of analytical wake models have been developed over the past 40 years (see, for instance, the review articles by Crespo *et al.* [3], Göçmen *et al.* [4], Porté-Agel *et al.* [5] and the references therein).

The bulk of these models share the same principle. The wake is divided into its near and far regions. The former is modeled using an inviscid actuator disk analysis and sets the boundary condition for the latter, which is modeled using arguments borrowed from the theory of self-preserving turbulent wakes [6]. A critical assumption is that the pressure in both of those regions does not deviate from its ambient value p_o. This can be thought to be approximately true when the turbine's induction factor (its effective solidity) is low. Indeed, most modern wind turbines operate at sufficiently low induction regimes, rendering the use of these models justified.

Situations arise, however, where the turbine operates at relatively high induction states. These might occur when the tip-speed ratio of the turbine assumes high values or in nonstandard turbine designs, as, for instance, in vertical axis wind turbines [7,8] or highly loaded horizontal axis wind turbines [9,10] (e.g., with multiple or very wide blades). In such cases, the turbine reaches a state where the wake pressure lowers significantly (a phenomenon also called base suction), rendering conventional wake models prone to failure.

The emergence of base suction sets a firm upper bound to the permissible induction factors of conventional wake models. In practice, however, the bound can be stricter than the one imposed by base suction, as an additional complication may arise when trying to enforce conservation of momentum in the wake. The momentum budgets that wake models employ are valid either very

*k.steiros13@imperial.ac.uk

close to the turbine (near region) or very far from the turbine (far region). Their coupling may be incompatible when a critical induction factor is exceeded. An additional constraint is thus set, which may be interpreted physically as the turbine having sufficiently low effective solidity, so the flow is only minimally perturbed, leading to marginally different physics in the near and far wake regions.

It is perhaps instructive to give some numbers to the above constraints. The induction factor is defined as $\alpha = 1 - u_t/U_o$, where u_t is the spatially averaged flow velocity through the turbine and U_o the free stream velocity. The base suction constraint sets an upper limit for α around 0.3–0.4 [10,11], while the coupling constraint in the widely popular Frandsen family of momentum-conserving models [12,13] sets a stricter upper limit of $\alpha = 0.25$.

There are, however, ways to circumvent the coupling constraint. One way is by relaxing the momentum conservation principle in the far wake. This is the approach followed in the model of Jensen [14] and its variants, which produce robust predictions at the cost of diminished accuracy. Another way is to use an entrainment-based closure of the far wake [15–17], which is capable of producing sensible solutions at the whole extent of the wake without having to sacrifice the fundamental physics of the problem. Still, these representations do not account for base suction in the wake.

In the present paper, we address both issues and derive a generalized turbine wake model that is not subject to the above two constraints (coupling and base suction). In the near wake, we circumvent the base-suction constraint by substituting the classical theory of Rankine-Froude (which assumes wake pressures equal to the ambient) with a generalized version of it [18,19], which takes into account base suction. In the far wake, we circumvent the coupling constraint by employing an entrainment-based representation [15,16] which we first extend so it also includes the effects of base suction. The result is an analytical turbine wake model which is equally accurate to conventional ones at low induction factors but continues to be accurate even at higher (in principle, for all, if vortex shedding is absent) induction factors, where other models break down.

The structure of the paper is as follows. Section II describes the flow solver which is used to provide reference data. Section III presents the derivation of the analytical turbine wake model. The predictions of the proposed model are compared against those of a well-established wake model and numerical simulations of the flow around model wind turbines in Sec. IV. Finally, Sec. V summarizes and concludes the paper.

II. NUMERICAL METHODOLOGY AND SETUP

The predictions of the developed model are tested against data from a series of large-eddy simulations (LESs) of the flow around model wind turbines. To this end, we use XCOMPACT3D (previously INCOMPACT3D/WINC3D), a well-established finite-difference framework that uses high-order compact schemes (sixth in the present paper) to solve the incompressible (filtered) Navier-Stokes equations [20–22]. XCOMPACT3D was recently extended and applied to the study of wind turbines and their wakes [23,24]. The wind turbines can be modeled by the actuator line or the actuator disk method; in the present paper, we use the former approach. The Smagorinsky model is used to model the effects of the unresolved fluid motions. Finally, a third-order Runge-Kutta method is used for time integration.

The configurations under consideration loosely follow the experiments of the "Blind Test 1" (BT1) workshop [25]. XCOMPACT3D has been previously used to study this particular problem, showing good agreement with the experimental results (for details, see Deskos *et al.* [23]). The BT1 experimental configuration is replicated in this paper as well, with the resolution that will be used for the simulations in the main body of this paper. Figure 1 shows the predicted wake velocity profiles at a horizontal cut at the hub height at different distances downstream of the turbine, and compares them with the available experimental measurements. Good agreement between the two sets of results can be observed, except in the vicinity of the tower (which, however, will not be considered in the simulations that follow) at the location immediately downstream of the turbine ($x/D = 1$).

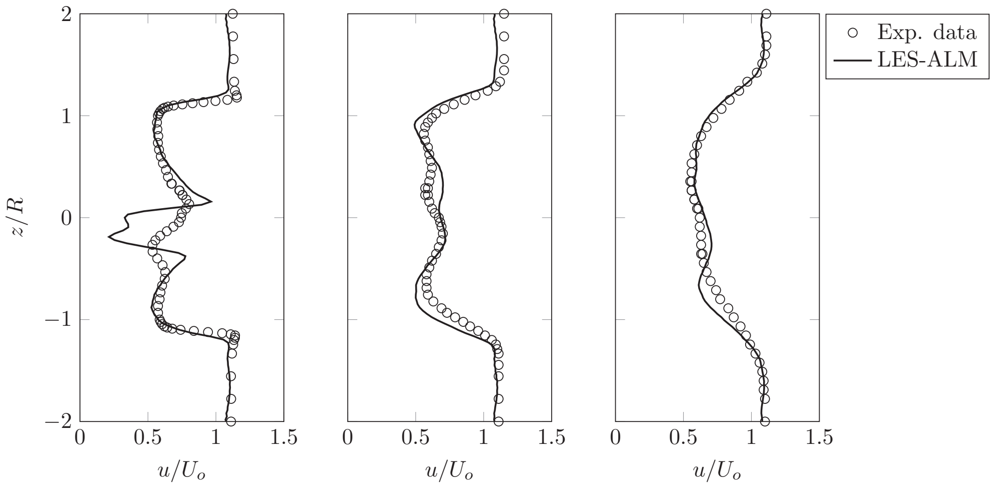

FIG. 1. Mean streamwise velocity profiles at a horizontal cut at the hub height at different distances downstream of the turbine, (left) $x/D = 1$, (middle) $x/D = 3$, and (right) $x/D = 5$. Numerical simulations (solid lines), experimental data (markers) [25].

For the comparison with the model that is derived in Sec. III, we consider an enlarged channel (compared with the BT1 experiments) to reduce blockage effects. The modified channel has a cross section spanning four turbine diameters in both spanwise and vertical directions, and runs 12 turbine diameters long. This results in a blockage ratio (defined as the ratio of gross turbine area and channel cross section) below 5%. Free-slip conditions are used at the channel walls, and laminar inflow is set at the inlet (very low turbulence levels, $I \simeq 0.3\%$, were present in the experiments). The model wind turbine is constructed based on the description and data given in Krogstad and Adaramola [26] and Krogstad and Eriksen [25], and is placed at the center of a vertical plane $x = 3.5D$ downstream of the inlet. The turbine operates at a constant tip speed ratio TSR = 6. A uniform grid consisting of $721 \times 241 \times 241$ points is used (resulting in a mesh of size $\simeq 42 \times 10^6$ points); this resolution can be considered sufficient for the purposes of this paper (see also Fig. 1), particularly since we will be considering the first moment of velocity only. Each blade/actuator line is discretized with 52 elements and no tower or nacelle is present to allow comparisons with the proposed analytical model. Simulations are run for a total time corresponding to more than 200 turbine rotations, with statistics extracted over the last $\simeq 85$. The wake boundaries are detected as the locations where the velocity is 0.95 times the free stream velocity, and the induction factor is obtained by computing the rotor-averaged mean streamwise velocity at the turbine plane.

High induction states are accessed by changing the turbine's number of blades. These regimes could also be accessed by changes in the geometry of the turbine or its rotational speed, or by reducing the free stream velocity. Out of the above options, we opted for changing the number of blades, as fewer modifications in the setup were required. Three different simulations are thus performed; one with the model three-bladed turbine described in Refs. [25,26], labeled T1, and two with its six- and nine-bladed variants, labeled T2 and T3, respectively. The induction factors were measured as $\alpha = 0.279$, 0.467, and 0.569, respectively.

III. DERIVATION OF THE MODEL

A. Near wake

The first few diameters of a high Reynolds number turbine wake are customarily modeled using inviscid flow theory. The rationale here is that at such small downstream distances, the

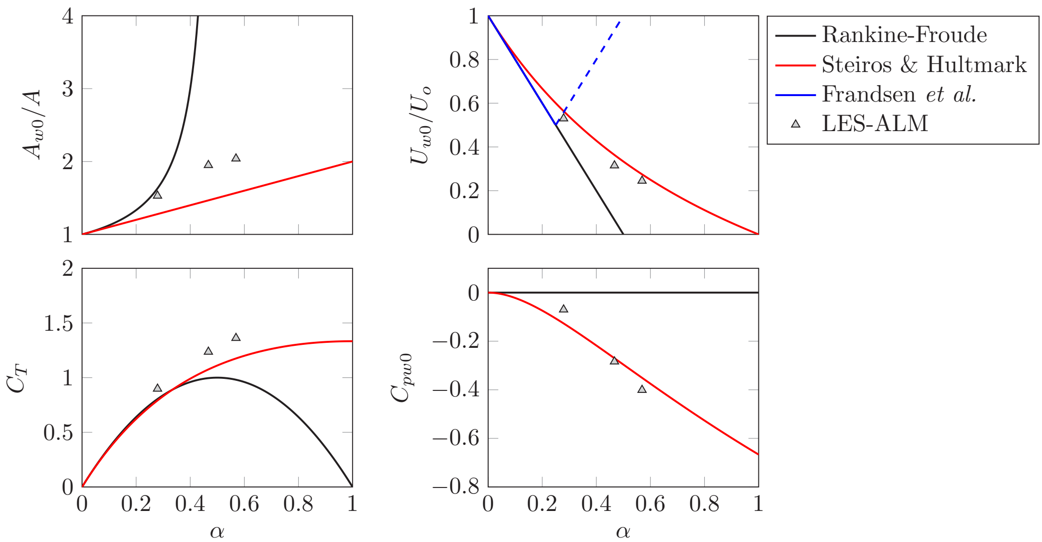

FIG. 2. Wake area (top left) and characteristic velocity (top right) after initial expansion, turbine thrust coefficient (bottom left), and pressure coefficient (bottom right) as a function of the induction factor α. Predictions of the theories of Rankine-Froude (black) and Steiros and Hultmark [18] (red). Included also are the wake velocity predictions of the model of Frandsen *et al.* [12] (blue), and data from numerical simulations (markers).

turbulent/shear stresses are cumulatively small compared to the effect of the initial wake expansion, and therefore do not significantly affect the flow quantities of the wake (see also relevant discussions in Refs. [19,27]). The near region typically spans about two turbine diameters downstream of the turbine [12]. In practice, however, most turbine wake models (e.g., Refs. [12–14,16]) assume that it is negligible. The main function of the near region is thus to impose the boundary condition on the far wake description that follows.

The basis of the inviscid analysis is the classical Rankine-Froude theory [11]. As mentioned in the Introduction, this theory neglects base-suction effects, thus limiting its applicability to low induction factors. Figure 2 shows the predictions of Rankine-Froude theory for the wake area A_w and characteristic velocity U_w after the initial expansion (denoted with the subscript 0), as well as for the thrust coefficient C_T. For completeness, these expressions are given below:

$$\frac{A_{w0}}{A} = \frac{1-\alpha}{1-2\alpha}, \quad \frac{U_{w0}}{U_o} = 1 - 2\alpha, \quad C_T = 4\alpha(1-\alpha), \tag{1}$$

where $A = \pi D^2/4$ is the turbine area. At an induction factor of $\alpha = 0.5$, the wake is unrealistically predicted as infinite and stagnant, while for larger induction factors the theory predicts negative wake velocities and areas (i.e., a complex wake characteristic size), and decreasing thrust. $\alpha = 0.5$ thus sets a mathematical base-suction upper limit, but we note that Rankine-Froude theory predictions are already inaccurate for induction factors larger than approximately $0.3 - 0.4$ [11].

We reiterate that the stricter coupling constraint has to be added to the above restriction when considering the momentum-conserving model of Frandsen *et al.* [12] and its variants. In particular, Frandsen *et al.* [12] derived $U_{w0}/U_o = 0.5 + 0.5\sqrt{1 - 8\alpha(1-2\alpha)}$ for the very near wake. This expression needs to be consistent with the original prediction of the Rankine-Froude theory. However, Fig. 2 shows that the two predictions agree only when $\alpha \leqslant 0.25$ thus limiting, in principle, the applicability of the models of the Frandsen family to low-induction regimes.

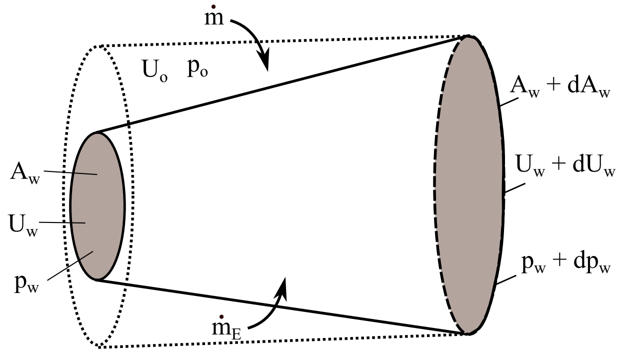

FIG. 3. Infinitesimal segment of the wake (solid lines) and outer control volume (dotted lines) where mass and momentum budgets are applied.

In the current paper, we substitute the Rankine-Froude theory of the near wake with the inviscid theory of Steiros and Hultmark [18], itself an extension of the porous flat plate theory of Taylor [28]. Using a seemingly different methodology, Taylor produced identical predictions to Rankine-Froude; the two theories can be thus thought equivalent. Steiros and Hultmark [18] proposed a correction to the Taylor model by imposing continuity and adding the effect of base suction, leading to the following expressions for the wake area and characteristic velocity after the initial expansion, as well as for the thrust and pressure coefficients:

$$\frac{A_{w0}}{A} = 1 + \alpha, \quad \frac{U_{w0}}{U_o} = \frac{1-\alpha}{1+\alpha}, \quad C_T = \frac{4\alpha(3-\alpha)}{3(1+\alpha)}, \quad C_{pw} = -\frac{8}{3}\left(\frac{\alpha}{1+\alpha}\right)^2. \tag{2}$$

The reader is referred to the original publication for more details on the assumptions and derivation of the Steiros and Hultmark [18] model. Figure 2 shows that the above expressions provide sensible, monotonic results for the whole range of induction factors. The same figure also includes data extracted from the numerical simulations (presented in Sec. IV), which correspond to the location immediately after the initial expansion (approximately one diameter downstream of the turbine). The data show that the model of Ref. [18] captures the initial wake properties more faithfully compared with the theory of Rankine-Froude, when the induction factor assumes high values.

B. Far wake

In the far wake, the turbulent stresses can no longer be neglected and, as a result, the wake continually expands. We model this expansion by using an entrainment-based closure, as it bypasses the coupling constraint that was previously discussed. Our entrainment-based representation is based on the work of Morton [15], with the difference that Morton only considered the very far wake case where pressure has regained its ambient value, i.e., $p_w = p_o$. Here, we require an estimate for the whole extent of the wake—even close enough to the turbine where $p < p_o$. We therefore need to extend Morton's theory to account for base suction.

1. Momentum integral

Consider the idealized segment of the turbulent wake shown in Fig. 3. The solid lines mark the turbulent-nonturbulent interface which we refer to as the wake boundary. Outside the wake, the velocity and pressure assume their ambient values U_o and p_o, while inside the wake the velocity assumes profiles which may be modeled as Gaussian [6,29]. Here, for simplicity, we assume a top-hat velocity profile (much like Morton [15] and Frandsen *et al.* [12]), and expect that this will not introduce large inaccuracies, given that we consider integral quantities. Mass conservation inside the wake-segment yields

$$\dot{m}_E = \rho d(U_w A_w), \tag{3}$$

where $d(\cdot)$ is a differential and $\dot{m}_E$ is the mass flux due to entrainment, which will be later estimated using the entrainment hypothesis. A combination of Eq. (3) with mass conservation inside the dotted control volume yields the following expression for the mass flux $\dot{m}$:

$$\dot{m} = \dot{m}_E - \rho U_o dA_w. \tag{4}$$

By applying momentum conservation in the dotted control volume and noting that in the outer flow the Reynolds stresses are negligible, we obtain

$$d\left(\rho U_w^2 A_w\right) = U_o \dot{m}_E + d(A_w(p_o - p_w)). \tag{5}$$

In the above equation and in the analysis that follows, the effect of the axial Reynolds stress term is not considered, as its role in the momentum budget can be neglected (see Appendix A). By combining the above with Eq. (3) and integrating, we obtain

$$\rho U_w A_w (U_o - U_w) + A_w (p_o - p_w) = T. \tag{6}$$

The first term on the left-hand side is the momentum deficit flux of the wake, while the second is the pressure deficit net force. Thus, the constant of integration T must be the thrust of the turbine. Equation (6) shows that our analysis is momentum conserving (in contrast to the Jensen [14] model and its variants), whether we consider the near or the far wake. In the special case of the very far wake, we have $p_w \approx p_o$ and Eq. (6) reduces to the well-known momentum integral for bluff bodies [6].

2. *Wake pressure and entrainment*

Our model's predictions rely on being able to solve Eq. (5). To do that, we first need to model the mass flux $\dot{m}_E$ and the pressure deficit $p_o - p_w$.

The mass flux $\dot{m}_E$ is due to turbulent mixing or entrainment of ambient fluid. This can be modeled using the entrainment hypothesis which states that the fluid outside the turbulent region crosses the turbulent interface with an entrainment velocity $u_e = E(U_o - U_w)$ [15], where the entrainment constant E needs to be empirically determined. Therefore, the mass flux due to entrainment at the wake segment of Fig. 3 is

$$\dot{m}_E = \rho E (U_o - U_w) \pi D_w dx. \tag{7}$$

The pressure deficit term needs to be expressed as a function of mean flow variables and our turbulence closure expression, i.e., the entrainment velocity u_e. Consider the annular control volume shown in Fig. 4, which is crossed by the wake boundary (red line). Above the wake boundary, the flow is assumed unperturbed and potential, and inside the wake boundary, turbulent. The velocity which crosses the wake boundary is assumed to be that of the outer flow U_o.

The control volume is bounded by two streamlines. When outside of the wake, they remain parallel (as the velocity between them is constant and equal to U_o), with negligible Reynolds stresses. After crossing the wake boundary, the Reynolds stresses become non-negligible, and the term $\overline{u_r' u_x'}$ continually transports momentum to the core of the wake. As a result, the streamlines converge toward the center due to mass conservation. The velocity inside the wake is U_w.

Given the above, we may derive an expression for the entrainment velocity u_e, which is defined as the velocity normal to the wake boundary. Therefore, $u_e = U_o \sin\hat{\theta}$, with $\hat{\theta} = \arctan \frac{1}{2}\frac{dD_w}{dx}$. For small wake expansion angles $\hat{\theta}$ (this was verified to hold in our simulations), we obtain

$$\frac{u_e}{U_o} = \frac{1}{2}\frac{dD_w}{dx}. \tag{8}$$

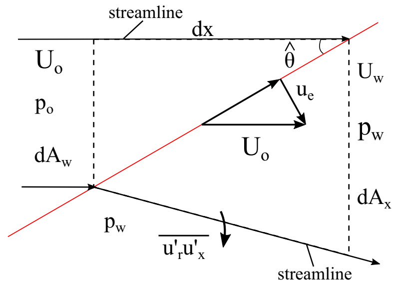

FIG. 4. Section of the annular control volume at the wake boundary. The red line represents the turbulent/nonturbulent interface. The control volume is bounded by two streamlines (black lines), which are initially parallel, but after entering the wake, they diverge.

Conservation of mass on the control volume yields $dA_x = \frac{U_o}{U_w} dA_w$, while conservation of momentum yields

$$\frac{p_o - p_w}{\rho} dA_w - \overline{u_x'^2} dA_w + U_o^2 dA_w = \overline{u_r' u_x'} \pi D_w dx + U_w^2 \frac{U_o}{U_w} dA_w. \tag{9}$$

Combining Eqs. (8) and (9) and noting that $dA_w = \frac{\pi D_w}{2} \frac{dD_w}{dx} dx$, we obtain

$$\frac{p_o - p_w}{\rho} = \overline{u_r' u_x'} \frac{U_o}{u_e} - U_o(U_o - U_w). \tag{10}$$

In the above equation, similar to Eq. (5), the axial Reynolds stress term is dropped, as its role compared to the velocity deficit term is negligible (see Appendix A). On the contrary, the shear Reynolds stress term is retained, as it is multiplied by U_o/u_e, rendering its effect at least an order of magnitude larger compared to that of the axial Reynolds stress term.

To proceed, we need to link the Reynolds stress $\overline{u_r' u_x'}$ with known quantities. Using an analogy with free shear flows, Tennekes and Lumley [6] proposed the expression $\overline{u_r' u_x'} \approx 0.4 \overline{u_r'^2}$ for the far wake; this is indeed close to experimental observations (see, for instance, Uberoi and Freymuth [30]). However, in the far wake it can be shown that $\rho \overline{u_r'^2} = p_o - p_w$ (see Tennekes and Lumley [6] for the planar wake and Appendix B for the axisymmetric wake). Combining the above expressions, we finally obtain our model for the pressure deficit term

$$\frac{p_o - p_w}{\rho U_0^2} = \frac{E(1 - U_w/U_o)^2}{0.4 - E + E U_w/U_o} \approx \lambda (1 - U_w/U_o)^2, \tag{11}$$

with $\lambda = 2.5E$. The approximation is most accurate for a combination of small E (typically close to 0.1), and $U_w \to U_o$. Equation (11) becomes asymptotically valid as the distance from the turbine increases. In Appendix C, we show that it provides a reasonably good approximation for the pressure term for the whole extent of the wake, increasingly so as the turbine induction factor (and therefore the importance of the pressure term in the budget equation) increases. We therefore use Eq. (11) for the whole extent of the wake. We are now in a position to derive the turbine wake model.

3. *Wake model*

Injecting Eq. (6) (for the wake area), (7) (for the entrainment mass flux), and (11) (for the wake pressure) into Eq. (5), and noting that $C_T = \frac{2T}{\rho U_o^2 A}$, with $A = \pi D^2/4$ being the turbine area, we obtain

$$\frac{d}{dx}\left[\frac{u^2 - \lambda(1-u)^2}{u(1-u) + \lambda(1-u)^2}\right] = \left(\frac{2}{C_T}\right)^{1/2} \frac{4E}{D} \left[\frac{1-u}{u + \lambda(1-u)}\right]^{1/2}, \tag{12}$$

where we have made the substitution $u = U_w/U_o$. Equation (12) can be integrated to yield

$$\frac{(4\lambda^2 - 5\lambda + 1)u^2 + (-8\lambda^2 + 8\lambda)u + 4\lambda^2 - 3\lambda}{(1-u)^{3/2}(\lambda + (1-\lambda)u)^{1/2}} = 6E\left(\frac{2}{C_T}\right)^{1/2}\frac{x - x_v}{D}, \tag{13}$$

where $\lambda = 2.5E$. In the case where $\lambda = 0$, pressure recovery is assumed to not affect the wake evolution, and Eq. (13) reduces to the standard far wake solution of Morton [15] and Luzzatto-Fegiz [16].

The constant of integration, x_v, expressed as a virtual origin, can be calculated by coupling the far wake solution of Eq. (13) with the near wake solution of Eq. (2). Indeed, for a particular turbine induction factor α, our near-wake inviscid model yields a prediction for the thrust coefficient C_T and the wake velocity after the initial expansion (see Sec. III A). The latter can be considered to occur at a small distance downstream of the rotor x_i, selected from a model for wake expansion. For simplicity, here we consider $x_i = 0$, as is typical for turbine wake models (e.g., Frandsen *et al.* [12], Jensen [14]). The only tuning parameter of the model is the entrainment constant E, which is known to be around 0.1 for turbulent wakes [15].

Having determined the wake velocity U_w, we can have an estimate for the wake area A_w using the momentum integral of Eq. (6) coupled with our closure for the wake pressure of Eq. (11), i.e.,

$$\frac{A_w}{A} = \frac{C_T}{2}[u(1-u) + \lambda(1-u)^2]^{-1}. \tag{14}$$

Equations (13) and (14) fully predict the wake development of a single wind turbine, and can be used in conjunction with wake-interaction models [5] to predict the flow field of an entire wind farm.

IV. WAKE MODEL VALIDATION

Figure 5 presents an assessment of the performance of the developed model at different induction regimes by comparing its predictions for the wake velocity, diameter, and pressure coefficient with the results of the numerical simulations and the predictions of the well-established, industry-standard model of Frandsen *et al.* [12]. In all cases, we take $E = 0.13$ for the presently developed model; this was the average value of E measured in the simulations (with a standard deviation of 0.035) and is within the range of values suggested by Morton [15] and Luzzatto-Fegiz [16]. The entrainment coefficient was found to be weakly depending on the turbine induction factor (coefficient of variation $\simeq 0.02$). However, slightly different values of E can be expected as the levels of stratification or background turbulence vary [31,32]. We note that the model does not consider, explicitly, the effects of stratification, Reynolds number, and background turbulence, which can be thought to be implicit in the empirical coefficient E. Appendix D presents a brief study on the sensitivity of the model to different values of E. For the model of Frandsen *et al.* [12] the wake spreading parameter was taken $k^* = 0.027$, which yielded a good fit to the numerical and entrainment model results.

The numerical simulations show that in all tested cases the wake initially expands rapidly, and the wake velocity accordingly drops. This trend continues until approximately one diameter downstream of the turbine, where the wake velocity assumes its lowest value. This is the location where the wake has concluded its initial expansion phase, marked with vertical dashed lines. Note that the values measured at this location are used in Fig. 2 when comparing the two near-wake theories with the simulation results. After this point, the wake expansion slows down considerably and the wake velocity continually increases; this corresponds to the far-wake region in the analytical models.

In the low induction case (T1), the predictions of both models are very similar for the wake velocity and wake diameter, and in qualitative agreement with the LES results. This is because the

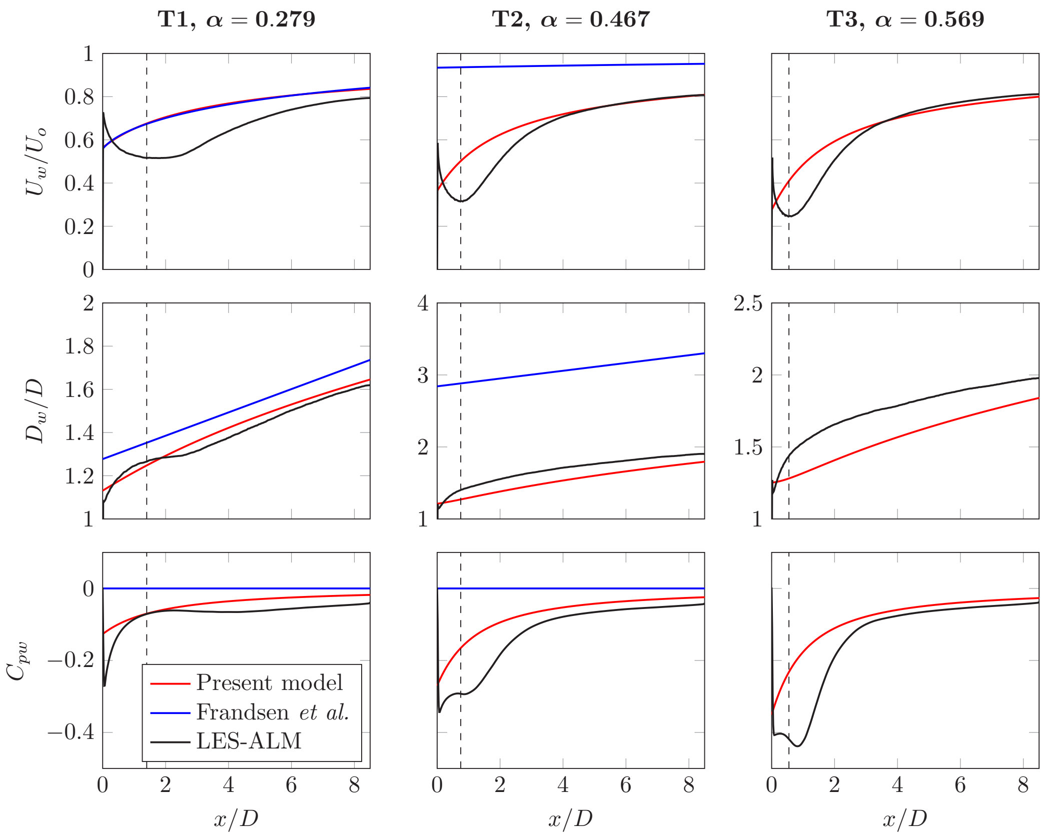

FIG. 5. Characteristic wake velocity (top), wake diameter (middle), and pressure coefficient (bottom) as a function of streamwise distance for turbines T1 (left), T2 (middle), and T3 (right). Numerical simulations (black), present model (red), Frandsen *et al.* [12] (blue). The dashed lines mark the end of the initial expansion phase of the wake.

induction factor is still small enough and base suction does not introduce appreciable effects. The presently developed model exhibits a slightly different prediction for the wake diameter due to its different initial condition. Neither of the two models is accurate very close to the turbine, as they both assume a negligible near-wake length (see discussion in Sec. III A). However, the far wake trends predicted by the models match those of the numerical simulation.

In the medium (T2) and high (T3) induction cases, the performance of the model of Frandsen *et al.* [12] is critically affected by the pressure and coupling constraints. In the T2 case, the initial condition is considerably far from the observations and, as a result, the overall wake evolution is unrealistic. In the T3 case, the model breaks down, predicting negative initial wake velocity and area. In contrast, the presently developed model remains consistent, producing sensible and qualitatively accurate predictions for the wake velocities and diameters, in both cases.

In all three tested cases, the prediction of the current model for the wake pressure coefficient is in relative agreement with the results of the numerical simulations. The agreement improves for larger downstream distances, given that pressure recovery is modeled using arguments for the very far wake. Conventional models (including Frandsen's) assume that the wake pressure is equal to the ambient. Our numerical results suggest that, for high induction factor rotors, this becomes approximately true only far from the turbine.

V. SUMMARY AND CONCLUSIONS

This paper introduced an analytical wake model for the prediction of the flow field downstream of wind turbines operating at arbitrary induction states. Similar to previous works [12,13,16], the turbine is represented as a porous plate, the effects of rotation are neglected, the wake is assumed axisymmetric, and its evolution is obtained using arguments from the theory of self-preserving turbulent wakes [6,15], setting the initial conditions from potential flow theory [18]. The main contribution of the present paper is the inclusion of the wake pressure evolution in the modeling. Whereas previous works assume a constant atmospheric wake pressure throughout the wake, here it is estimated via a combination of potential flow theory results, with an approximation which links pressure evolution and turbulent entrainment.

Comparison of the theoretical predictions with data from high-fidelity numerical simulations showed that the currently proposed model has similar accuracy to the Frandsen model at low induction factors but continues to be accurate at higher induction factors where conventional wake models either display deteriorating accuracy or even break down.

In the future, it would be interesting to extend the model by applying it to yawed conditions [33,34], by formulating a criterion for the determination of the near-wake length, or by implementing it within wake-farm modeling toolboxes to enable assessments of the collective behavior of highly loaded turbines within a wind farm.

ACKNOWLEDGMENTS

We would like to thank Dr. Sylvain Laizet for helpful discussions on the use of the XCOMPACT3D framework. N.B. was supported by EPSRC Grant No. EP/V000942/1. K.S. was supported by Imperial College London via a Junior Research Fellowship.

Both authors contributed equally to this work.

APPENDIX A: AXIAL REYNOLDS STRESS

At the far wake, the pressure and axial Reynolds stress terms are both negligible compared to the momentum deficit term, as shown by the order-of-magnitude analysis of Tennekes and Lumley [6]. For that reason, inclusion or not of the pressure and/or Reynolds stress terms in the far wake does not substantially affect the momentum budget [Eq. (5)]. Near the bluff body, however, the situation is different; there are indications that the Reynolds stress term is negligible there, but the pressure term is not (several potential flow models, e.g., Steiros and Hultmark [18], Yeung and Parkinson [35], provide reliable predictions of the near field by including the wake pressure but neglecting the Reynolds stresses).

The above are tested using data from one of our LESs (case T2, $\alpha = 0.467$). In Fig. 6, we plot the momentum deficit flux $U_w(U_o - U_w)$, the pressure deficit $(p_o - p_w)/\rho$, and the axial Reynolds stress $\overline{u_x'^2}$ along the streamwise distance x/D (note that these are to a degree affected by blockage and the omission of tower and nacelle in the modeling of the turbine). It can be seen that in the near wake, the axial Reynolds stress term is much smaller compared to the momentum and pressure deficit terms, and may thus be neglected. In the far wake, we observe that both the pressure and Reynolds stress terms tend to zero, i.e., both can be safely neglected from the momentum budget, as is long known from classical turbulence studies (see Refs. [6,15]).

We note that the Reynolds stress term cannot be currently modeled, but its inclusion is expected to only act as a small correction to the existing pressure term. The latter is retained throughout the wake, even far from the body, where it could be neglected as it no longer affects the evolution of the wake. The reason for that is that if it is suddenly removed, this would lead to a discontinuity and a piecewise analytical solution, which would only increase the complexity of the theory. We finally note that, even if one is interested in the far wake only, it is still important to take into account

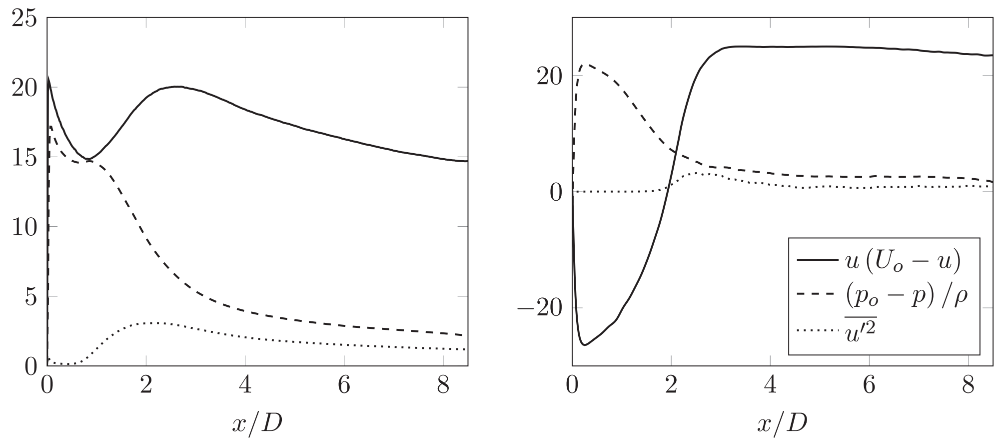

FIG. 6. Momentum deficit (solid), pressure (dashed), and axial Reynolds stress (dotted) along streamwise distance, case T2. The terms are averaged in the wake (left) and extracted at the center line (right).

the pressure in the first few diameters downstream of the turbine, as the initial pressure-dominated region acts as a initial condition which determines the later evolution of the wake.

APPENDIX B: RADIAL REYNOLDS STRESS

Under the assumptions of stationarity and statistical axisymmetry, the radial component of the Reynolds-averaged Navier Stokes equations projected on a cylindrical coordinate system, and neglecting viscous stresses, becomes

$$rU_r\frac{\partial U_r}{\partial r} + rU_x\frac{\partial U_r}{\partial x} + \frac{\partial r\overline{u_r'^2}}{\partial r} + r\frac{\partial \overline{u_r'u_x'}}{\partial x} - \overline{u_\theta'^2} = -\frac{r}{\rho}\frac{\partial \overline{p}}{\partial r}.$$

The far wake is slender, i.e., $\partial/\partial x \ll \partial/\partial r$. Then, following an order-of-magnitude analysis similar to the one of Tennekes and Lumley [6], and using the continuity equation in cylindrical coordinates, we find that, at first-order approximation, the above equation reduces to

$$\frac{\partial \overline{u_r'^2}}{\partial r} + \frac{\overline{u_r'^2} - \overline{u_\theta'^2}}{r} = -\frac{1}{\rho}\frac{\partial \overline{p}}{\partial r}.$$

By integrating from r to infinity, the above becomes

$$\overline{u_r'^2} + \frac{\overline{p}}{\rho} - G(r) = \text{const},$$

where $G(r) = \int_r^\infty \frac{\overline{u_r'^2} - \overline{u_\theta'^2}}{r'}dr'$. However, $\overline{u_r'^2} \approx \overline{u_\theta'^2}$ in the far axisymmetric wake [30], and thus the effective spatial average $G(r)$ is negligible. Furthermore, $\overline{u_r'^2}$ is negligible for $r \to \infty$, where the pressure assumes its ambient value p_o. The above equation then becomes

$$\rho\overline{u_r'^2} = p_o - \overline{p},$$

which is the same result that Tennekes and Lumley [6] derived for planar wakes.

APPENDIX C: WAKE PRESSURE MODEL VALIDATION

The validity of our model for the wake pressure, i.e., Eq. (11), is assessed using data from the numerical simulations (for details, see Sec. II). Figure 7 plots the pressure downstream of the three

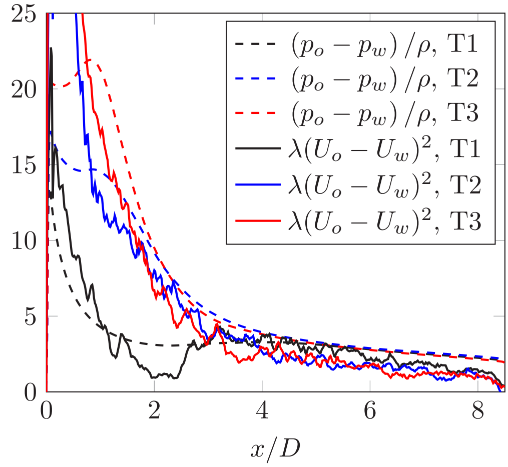

FIG. 7. Pressure deficit (dashed) and model expression for it (solid) as a function of streamwise distance, integrated in the wake of the simulated wind turbines T1 (black), T2 (blue), T3 (red), corresponding to induction factors $\alpha = 0.279$, 0.467, and 0.569, respectively.

turbines, $(p_o - p_w)/\rho$, along with the approximate expression for it, $\lambda(U_o - U_w)^2$. In the latter, the entrainment coefficient is calculated as $E = \sin\left(\arctan\left(\frac{1}{2}\frac{dD_w}{dx}\right)\right)\frac{U_o}{U_o-U_w}$ (see Sec. III). Equation (11) is shown to be a reasonable approximation for the wake pressure, except for the region very close to the body, where the wake is yet to transition to turbulence, and the entrainment parametrization and far-wake assumptions cannot be expected to apply.

APPENDIX D: MODEL SENSITIVITY STUDY

Works in the literature (mainly for jets, plumes, and secondarily wakes) suggest that E takes values in the range $0.1 - 0.16$ [15,16]. In Fig. 8, we plot the predictions of the developed model for the two limit values listed above, i.e., $E = 0.1$ and $E = 0.16$; the uncertainty can be seen to increase with the turbine induction factor. Qualitatively, the expected behavior is recovered, where larger values for the entrainment coefficient E result in faster wake recovery.

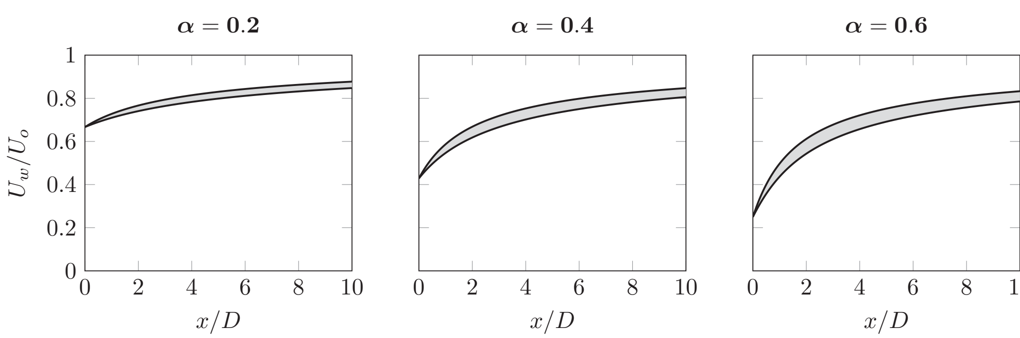

FIG. 8. Characteristic wake velocity as a function of streamwise distance, as predicted by the presently proposed model, for three different induction factors. The upper and lower solid lines are the model predictions for $E = 0.16$ and $E = 0.1$, respectively.

[1] N. G. Mortensen, L. Landberg, I. Troen, and E. Lundtang Petersen, Wind atlas analysis and application program (WAsP), Technical Report No. Risø-I-666(EN)(v.2), Risø National Laboratory, Denmark (1993).
[2] J. Annoni, P. Fleming, A. Scholbrock, J. Roadman, S. Dana, C. Adcock, F. Porte-Agel, S. Raach, F. Haizmann, and D. Schlipf, Analysis of control-oriented wake modeling tools using lidar field results, Wind Energy Sci. **3**, 819 (2018).
[3] A. Crespo, J. Hernandez, and S. Frandsen, Survey of modelling methods for wind turbine wakes and wind farms, Wind Energy **2**, 1 (1999).
[4] T. Göçmen, P. Van der Laan, P.-E. Réthoré, A. Peña Diaz, G. C. Larsen, and S. Ott, Wind turbine wake models developed at the technical university of Denmark: A review, Renewable Sustainable Energy Rev. **60**, 752 (2016).
[5] F. Porté-Agel, M. Bastankhah, and S. Shamsoddin, Wind-turbine and wind-farm flows: A review, Boundary Layer Meteorol. **174**, 1 (2020).
[6] H. Tennekes and J. L. Lumley, *A First Course in Turbulence* (MIT Press, Cambridge, MA, 1972).
[7] C. Simao Ferreira, H. A. Madsen, M. Barone, B. Roscher, P. Deglaire, and I. Arduin, Comparison of aerodynamic models for vertical axis wind turbines, J. Phys.: Conf. Ser. **524**, 012125 (2014).
[8] A. A. Ayati, K. Steiros, M. A. Miller, S. Duvvuri, and M. Hultmark, A double-multiple streamtube model for vertical axis wind turbines of arbitrary rotor loading, Wind Energy Sci. **4**, 653 (2019).
[9] J. N. Sørensen, W. Z. Shen, and X. Munduate, Analysis of wake states by a full-field actuator disc model, Wind Energy **1**, 73 (1998).
[10] D. P. Georgiou and N. G. Theodoropoulos, A momentum explanation for the unsatisfactory Betz model prediction in highly loaded wind turbines, Wind Energy **14**, 653 (2011).
[11] M. O. L. Hansen, *Aerodynamics of Wind Turbines* (Routledge, Oxon, 2015).
[12] S. Frandsen, R. Barthelmie, S. Pryor, O. Rathmann, S. Larsen, J. Højstrup, and M. Thøgersen, Analytical modelling of wind speed deficit in large offshore wind farms, Wind Energy **9**, 39 (2006).
[13] M. Bastankhah and F. Porté-Agel, A new analytical model for wind-turbine wakes, Renewable Energy **70**, 116 (2014).
[14] N. O. Jensen, A note on wind generator interaction, Technical Report No. Risø-M No. 2411, Risø National Laboratory, Denmark (1983).
[15] B. R. Morton, On a momentum-mass flux diagram for turbulent jets, plumes and wakes, J. Fluid Mech. **10**, 101 (1961).
[16] P. Luzzatto-Fegiz, A one-parameter model for turbine wakes from the entrainment hypothesis, J. Phys.: Conf. Ser. **1037**, 072019 (2018).
[17] N. Li, Y. Liu, L. Li, H. Meng, S. Han, and J. Yan, A novel two-dimensional entrainment wake model for wind turbine wakes, Int. J. Green Energy, 1 (2021).
[18] K. Steiros and M. Hultmark, Drag on flat plates of arbitrary porosity, J. Fluid Mech. **853**, R3 (2018).
[19] K. Steiros, N. Bempedelis, and L. Ding, Recirculation regions in wakes with base bleed, Phys. Rev. Fluids **6**, 034608 (2021).
[20] S. Laizet and E. Lamballais, High-order compact schemes for incompressible flows: A simple and efficient method with quasi-spectral accuracy, J. Comput. Phys. **228**, 5989 (2009).
[21] S. Laizet and N. Li, Incompact3d: A powerful tool to tackle turbulence problems with up to $\mathcal{O}(10^5)$ computational cores, Int. J. Numer. Methods Fluids **67**, 1735 (2011).
[22] P. Bartholomew, G. Deskos, R. A. S. Frantz, F. N. Schuch, E. Lamballais, and S. Laizet, Xcompact3d: An open-source framework for solving turbulence problems on a cartesian mesh, SoftwareX **12**, 100550 (2020).
[23] G. Deskos, S. Laizet, and M. D. Piggott, Turbulence-resolving simulations of wind turbine wakes, Renewable Energy **134**, 989 (2019).
[24] G. Deskos, S. Laizet, and R. Palacios, Winc3d: A novel framework for turbulence-resolving simulations of wind farm wake interactions, Wind Energy **23**, 779 (2020).
[25] P.-Å. Krogstad and P. E. Eriksen, "Blind test" calculations of the performance and wake development for a model wind turbine, Renewable Energy **50**, 325 (2013).
[26] P.-Å. Krogstad and M. S. Adaramola, Performance and near wake measurements of a model horizontal axis wind turbine, Wind Energy **15**, 743 (2012).

[27] A. Roshko, Perspectives on bluff body aerodynamics, J. Wind Eng. Ind. Aerodyn. **49**, 79 (1993).
[28] G. I. Taylor, Air resistance of a flat plate of very porous material, Aeronaut. Res. Counc., Rep. Memo. **2236**, 159 (1944).
[29] M. Abkar, J. N. Sørensen, and F. Porté-Agel, An analytical model for the effect of vertical wind veer on wind turbine wakes, Energies **11**, 1838 (2018).
[30] M. S. Uberoi and P. Freymuth, Turbulent energy balance and spectra of the axisymmetric wake, Phys. Fluids **13**, 2205 (1970).
[31] E. Rind and I. P. Castro, On the effects of free-stream turbulence on axisymmetric disc wakes, Exp. Fluids **53**, 301 (2012).
[32] K. S. Kankanwadi and O. R. Buxton, Turbulent entrainment into a cylinder wake from a turbulent background, J. Fluid Mech. **905**, A35 (2020).
[33] M. Bastankhah and F. Porté-Agel, Experimental and theoretical study of wind turbine wakes in yawed conditions, J. Fluid Mech. **806**, 506 (2016).
[34] C. R. Shapiro, D. F. Gayme, and C. Meneveau, Modelling yawed wind turbine wakes: A lifting line approach, J. Fluid Mech. **841**, R1 (2018).
[35] W. W. H. Yeung and G. V. Parkinson, Base pressure prediction in bluff-body potential-flow models, J. Fluid Mech. **423**, 381 (2000).